Quantum Well States in Two-Dimensional Gold Clusters on MgO Thin Films

X. Lin, N. Nilius,* and H.-J. Freund
Fritz-Haber Institut der MPG, Faradayweg 4-6, D14195 Berlin, Germany

M. Walter,† P. Frondelius, K. Honkala, and H. Häkkinen‡
Departments of Physics and Chemistry, Nanoscience Center, University of Jyväskylä, P.O. Box 35 (YFL), FI-40014 Finland
(Received 11 November 2008; published 19 May 2009)

The electronic structure of ultrasmall Au clusters on thin MgO/Ag(001) films has been analyzed by scanning tunneling spectroscopy and density functional theory. The clusters exhibit two-dimensional quantum well states, whose shapes resemble the eigenstates of a 2D electron gas confined in a parabolic potential. From the symmetry of the highest occupied (HOMO) and lowest unoccupied molecular orbital (LUMO) of a particular cluster, its electron filling and charge state is determined. In accordance with a Bader charge analysis, aggregates containing up to 20 atoms accumulate one to four extra electrons due to a charge transfer from the MgO/Ag interface. The HOMO-LUMO gap is found to close for clusters containing between 70 and 100 atoms.

DOI: 10.1103/PhysRevLett.102.206801 PACS numbers: 73.21.La, 68.37.Ef, 68.47.Gh, 71.15.Mb

Ultrasmall metal clusters exhibit unique size-dependent properties due to a large fraction of surface atoms and a distinct electronic structure [1]. Reducing the atom count below a few hundred, the bulk band structure breaks down and discrete energy levels emerge. These quantization effects are in part responsible for the unusual chemical properties of small metal particles with respect to bulk materials [2–4], as well as for a variety of optical and electronic phenomena [1]. Experimentally, electron quantization effects are difficult to access, and the existing knowledge is mainly based on photoelectron spectroscopy on size-selected clusters in the gas phase [5,6]. Naturally, those experiments cannot account for substrate effects, which are, however, of pivotal importance for the electronic structure of supported metal particles [3,4,7]. The investigation of adclusters, on the other hand, is often hampered by their size and shape distribution on the surface, giving rise to inhomogeneous broadening effects in nonlocal spectroscopic techniques. Scanning tunneling microscopy (STM) provides a powerful alternative to study the interplay between geometric and electronic properties of supported clusters at the local scale. Using this technique, quantum well states have been detected in clusters of different dimensionality grown on metal [8,9], semimetal [10,11], and oxide supports [12].

This Letter reports a combined STM/density functional theory (DFT) study on Au clusters on MgO/Ag(001) thin films. MgO belongs to the best-explored oxide materials, as high-quality films can be prepared [13,14] and theoretical modeling is easy due to its simple rocksalt structure. Nanodispersed Au on MgO/Ag(001) follows a specific adsorption scheme, being governed by a charge transfer from the metal support into low-lying Au affinity levels [15–18]. The Au anions strongly bind to the MgO film, via an electrostatic attraction to the Mg^{2+} surface ions, a polaronic distortion of the oxide lattice, and the polarization of the metal underneath [15,17]. The recently observed formation of two-dimensional (2D) Au islands on MgO thin films [19,20], being in contrast to the 3D growth found on bulk MgO, has been taken as an indication for such electron transfer processes. However, direct experimental evidence for the negative charging of Au could not be provided in that case. This work gives detailed insights into the structural and electronic properties as well as the charge state of individual Au clusters on a 2 ML thin MgO film, exploiting the distinct symmetry of quantum well states in their confined electronic system.

The experiments are carried out with an ultrahigh vacuum STM operated at 4.5 K. The sample electronic structure is probed with differential conductance (dI/dV) spectroscopy using a lock-in technique ($V_{\mathrm{mod}} = 10$ mV rms). The MgO film is prepared by Mg deposition onto a sputtered and annealed Ag(001) surface in 1×10^{-6} mbar O_2 and at 570 K. It results in an atomically flat MgO film, exposing large rectangular terraces delimited by nonpolar step edges [13,16]. Single Au atoms are evaporated from a high-purity wire and deposited onto the sample at 100 K. Because of the thermal energy of the incoming atoms and their low diffusion barrier on the MgO, Au aggregates into ultrasmall clusters. The DFT calculations are performed with the grid-projector-augmented-wave method (0.2 Å grid spacing) [21] using the generalized-gradient approximation [22,23]. Periodic boundary conditions are applied in the surface plane, while the perpendicular direction is kept nonperiodic. The substrate is modeled with two MgO layers being in registry with three Ag(001) planes of 4.14 Å lattice constant. Except for the two bottom Ag layers, all atoms are relaxed during geometry optimization until forces are below 0.05 eV/Å. Depending on the cluster size, (4×4), (5×5), and (6×6) surface cells are constructed. A Monkhorst-Pack $2 \times 2 \times 1$ k-point sampling and the

Bader method [24] are used to analyze the electronic structure and the charge state of the adclusters. The STM images are simulated with the Tersoff-Hamann formalism [25], using a state density of 1.4×10^{-5} e/Å to match the experimental tunnel current of 5 pA.

Figure 1(a) shows an STM-topographic image of a 2 ML MgO film after deposition of 0.02 ML Au. The dominant surface species are round protrusions of 6–7 Å size and 0.8 Å height, being identified as Au monomers [19]. Additionally observed adstructures with 1D and 2D shapes and 0.8 Å height are assigned to single-layered Au clusters [26]. For selected 2D species, a sudden increase in apparent height occurs when the imaging bias is increased above a certain threshold [Fig. 1(b)] [27]. Simultaneously, the cluster appearance changes from the compact structures visible at low bias to characteristic flowerlike shapes [Fig. 1(c)] [18,25]. Both effects indicate that the STM contrast is now governed by electronic properties of the clusters, and quantum well states (QWSs) become available for electron transport between tip and sample. The QWSs give rise to pronounced maxima in the dI/dV spectra of the respective clusters, which occur at similar bias values as the contrast change in the images (Fig. 2). The highest occupied (HOMO) and lowest unoccupied molecular orbital (LUMO) are hereby usually separated by a region of zero conductance that varies between 0.1 and 1.8 eV for differently sized clusters. Conductance imaging performed at the dI/dV peak positions provides the spatial symmetry of the QWSs. In most cases, they are characterized by an irregular lobe pattern, manifesting the disordered arrangement of Au atoms within the aggregate [Fig. 1(c)]. In selected cases, also highly symmetric orbitals with a defined node structure are observed, which closely resemble the eigenstates of a free-electron gas confined in a 2D parabolic potential. According to the number of nodal planes, orbitals with S, P, D, F, and G symmetry, corresponding to an angular momentum quantum number of 0–4, can be distinguished. The free-electron nature of the QWSs in Au clusters reflects their origin from the Au 6s electrons that delocalize in the cluster potential, as already recognized in an earlier DFT study [18]. The initial orbital shapes are maintained in this case, because the Au 6s-derived states reside in the MgO band gap (6.4 eV for a 2 ML film) [14] and are well separated from the low-lying Au 5d band [23].

Based on the STM-topographic data and the orbital shapes, the true atomic and electronic structure of the Au clusters is determined with DFT, by searching for candidate clusters with matching properties. This is demonstrated for the cluster shown in Fig. 2. In low-bias images, the cluster adopts a pentagonal shape with 14 Å diameter. Above +0.7 V and below −0.3 V, flowerlike patterns with eight lobes and four nodal planes become visible, indicating a G symmetry of both frontier orbitals. Conductance data reveal an even more complex picture, where only the HOMO at −0.4 V and the LUMO at +0.8 V are of G character, while two additional peaks at −0.8 and −1.2 V show P symmetry with the node being orthogonal in both cases. The symmetry of the HOMO-1 slightly interferes with the HOMO, which still controls the integral conductance of the junction and therefore the tip-sample distance. Consequently, artificial maxima appear in the dI/dV maps of the HOMO-1 at the node positions of the HOMO. All images reveal a certain difference between

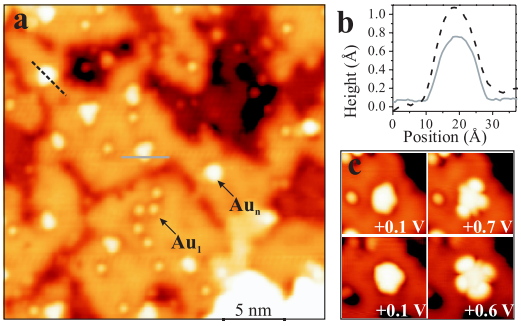

FIG. 1 (color online). (a) STM image of Au atoms and clusters on 2 ML MgO/Ag(001) ($U_s = 0.4$ V, $I = 5$ pA, 26×26 nm^2). (b) Line profiles of the two clusters depicted by the solid and dashed lines in (a). The first cluster appears lower due to the absence of QWSs below the scan bias. (c) Topographic images of an asymmetric and a symmetric Au cluster taken in the HOMO-LUMO gap (left) and above the LUMO position (right) (5.5×5.5 nm^2).

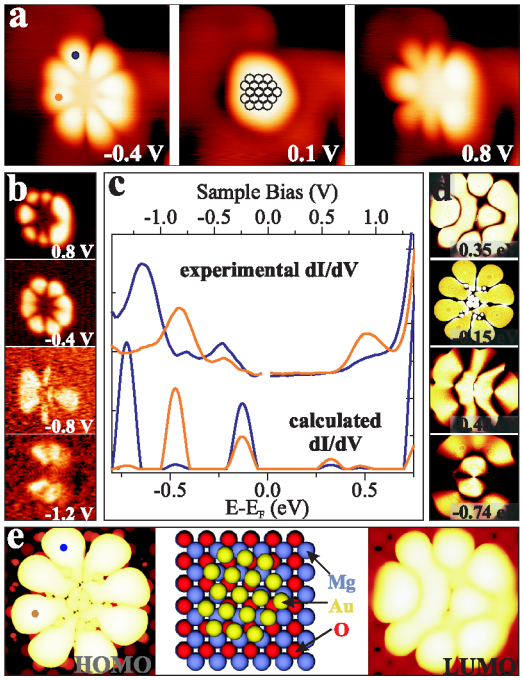

FIG. 2 (color online). (a) STM-topographic and (b) conductance images of an Au_{18} cluster on 2 ML MgO/Ag(001) ($I = 5$ pA, 3.9×3.9 nm^2) in comparison with simulated (d) conductance and (e) topographic images (2×2 nm^2) and a structure model. (c) Experimental and simulated dI/dV spectra taken at the blue and orange dots marked on the cluster in (a) and (e).

the left and the right cluster half, indicating a slight asymmetry of its atomic configuration.

After an extensive DFT screening, a planar Au_{18} cluster with D_{2h} symmetry was found to perfectly reproduce the experimental results of Fig. 2. Its structure is derived from a D_{6h}-symmetric Au_{19} cluster with one corner atom removed, giving rise to the pentagonal shape [23]. The Au_{18} cluster has 11 occupied valence states, ten of them filling the first four electronic shells of the harmonic potential [Fig. 3(c)]. The HOMO and LUMO therefore correspond to the lowest and second lowest orbital of the 5th shell, respectively, and are both of $1G$ character. The slight asymmetry in the atomic configuration lifts the degeneracy of both states and gives rise to a HOMO-LUMO gap. It also induces the lower state density of the LUMO at the position of the missing atom. Both results, the G character of the frontier orbitals and the asymmetric LUMO, perfectly match the experimental results. The agreement is further supported by the calculated symmetry of the HOMO-1 and HOMO-2 of the Au_{18}, which are the two orthogonal $2P$-QWSs in the 4th electronic shell. Also dI/dV spectra have been simulated by calculating the bias-dependent Tersoff-Hamann tunneling current and taking the numerical derivative [Fig. 2(c)]. The sequence of states and even their intensity modulation within the cluster agree well with the experiment, although the peak energies and the HOMO-LUMO gap are underestimated due to the well-known DFT "band-gap problem."

The filling of 11 QWSs fixes the number of valence electrons in the Au_{18} cluster with 22. Each of the 18 Au atoms donates its $6s$ electron to the QWSs, implying that the missing four electrons have been transferred from the support. The presence of four excess charges is corroborated by the computed Bader charge of $-3.54|e|$ or $-0.2|e|$ per atom, similar to the result obtained for a compact Au layer on 2 ML MgO/Ag(001). The characteristic orbital structure of Au_{18} therefore provides clear evidence for the negative charging of the adcluster and enables the first reliable quantification of the underlying electron transfer from the MgO/Ag interface [15–17,20].

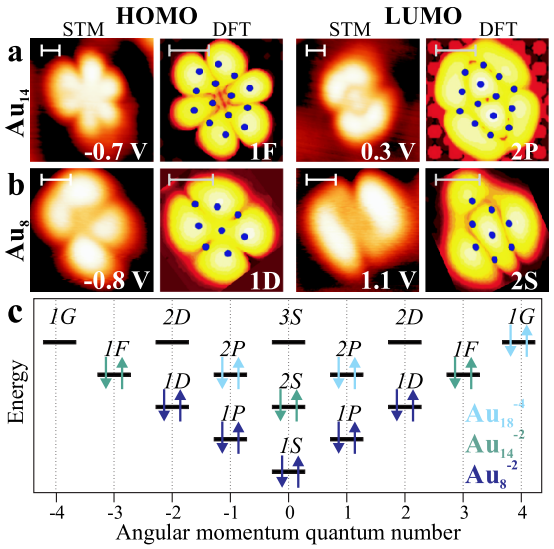

FIG. 3 (color online). (a),(b) Measured and calculated HOMO and LUMO shapes for two Au clusters. The dots in the calculated images depict the Au positions. All scale bars are 5 Å. (c) Orbital filling in the harmonic oscillator model for the clusters shown in (a), (b), and Fig. 2.

The concept of reconstructing the atomic structure of Au clusters on MgO films has been applied to other examples, aiming for more general conclusions on their size-dependent properties. Figure 3(a) shows a slightly smaller aggregate, where the HOMO is of F symmetry and the LUMO, 1.0 eV higher in energy, has P character. Comparing this to DFT results of various candidate clusters, best matching is achieved for a D_{4h}-symmetric Au_{14}. The Bader analysis reveals that this cluster carries two transfer electrons from the support, bringing the total electron count to 16. This charge state is compatible with the level occupancy predicted by the harmonic oscillator model. The HOMO is the 8th QWS and has $1F$ character, while the LUMO is of $2P$ symmetry as in the experiment [Fig. 3(c)]. The smallest cluster with well-defined QWSs in this study has frontier orbitals of D and mixed S and P character, separated by an energy gap of 1.9 eV [Fig. 3(b)]. The underlying configuration is assigned to a twofold negatively charged Au_8 cluster, whose HOMO and LUMO are the $1D$ and $2S$ QWS in the harmonic potential, respectively. Whereas the calculated HOMO matches perfectly, the LUMO symmetry slightly differs from the experiment. The deviations might be explained by a certain overlap between the LUMO and the $2P$-like LUMO + 1, emphasizing the two outer lobes in the measurement. In all Au clusters, QWSs with higher angular momentum in a given shell are found to be lower in energies than their S- and P-like counterparts, in contrast to the ideal oscillator model. This finding indicates a certain admixture of box character to the harmonic potential, introducing a downshift of states with higher angular momentum [6].

In Fig. 4(a), the evolution of the HOMO-LUMO gap (E_g) is analyzed for clusters of different atom counts, being estimated from the cluster area Ω measured in the STM. Spectroscopy reveals a gradual closing of the gap around E_F until metallic behavior sets in for 70–100 atoms per cluster [2,4]. The gap size follows the inverse cluster area (dashed line), as expected for the energy separation of eigenstates in a 2D harmonic or spherical box potential [6]. The smooth dependence of the gap size on Ω is superimposed by oscillations that reach 0.8 eV for ultrasmall clusters. Large E_g values hereby suggest electronic shell closing, whereas smaller gap sizes are compatible with open-shell configurations. A clear oscillatory pattern, as predicted for a harmonic oscillator [18], is not observed, as nonsymmetric Au clusters are abundant, in which the degeneracy of QWSs is lifted. Furthermore, energetically unfavorable, open-shell clusters might be suppressed on the MgO surface, e.g., by rearranging their atomic con-

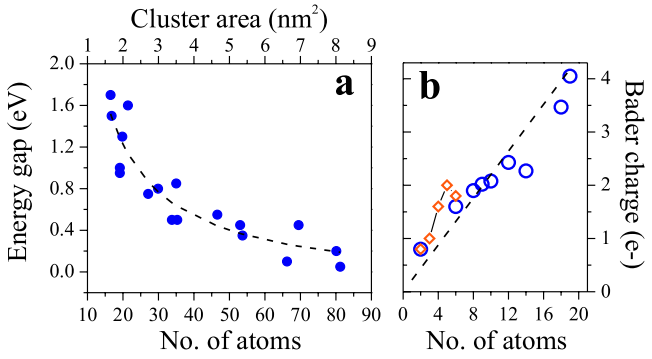

FIG. 4 (color online). (a) Experimental HOMO-LUMO gap for different Au clusters. The atom number is approximated from deconvoluted STM images, using the DFT results as a reference. The dashed line is a fit of the data to the inverse cluster size. (b) Calculated number of excess electrons in linear (diamonds) [26] and 2D Au clusters (circles) on 2 ML MgO/Ag(001). The line depicts the charge accumulation of $-0.2|e|$ per atom, as computed for a compact Au layer on 2 ML MgO/Ag(001).

figuration, attaching further atoms, or adapting the charge transfer from the support to enforce shell closing.

The electron transfer into the Au clusters is with $-0.2|e|$ per atom nearly proportional to the atom number in the investigated size range [Fig. 4(b)]. Interestingly, the accumulated charge is lower in 2D than in 1D aggregates for small atom counts, manifesting a better delocalization of the transfer electrons and a reduced internal Coulomb repulsion in the linear configuration [26]. This effect diminishes for clusters containing more than 7–8 atoms, when the 2D growth of Au becomes energetically favorable [12,26].

In conclusion, QWSs with distinct symmetries have been observed in 2D Au clusters on MgO/Ag(001) thin films. For sufficiently symmetric clusters, the QWSs resemble the free-electron states in a 2D parabolic potential, as mainly the Au 6*s* orbitals are involved in the quantization phenomenon. In those cases, the distinct HOMO and LUMO symmetries are exploited to deduce the atomic configuration, the electron filling, and the charge state of the clusters. An accumulation of excess electrons is revealed with increasing cluster size, verifying the long-debated charge transfer mechanism on the MgO/Ag system. Our STM-DFT study is able to connect the geometric and electronic properties of individual metal clusters on oxide supports, contributing to the analysis of the unique chemical behavior of such material systems.

This work is supported by the A. v. Humboldt foundation (X. L.), the Academy of Finland (M. W., P. F., K. H., H. H.), the DFG (M. W.), and the COST D41 network. We thank CSC (Espoo, Finland), FZ Jülich, and EU DEISA for providing the computer resources.

*Corresponding author.
nilius@fhi-berlin.mpg.de
†Present address: Fakultät für Physik, Universität Freiburg, S. Meier Straße 21, D79104 Freiburg, Germany.
‡Corresponding author.
Hannu.J.Hakkinen@jyu.fi

[1] *Metal Clusters*, edited by W. Ekardt (Wiley, Chichester, 1999).
[2] M. Valden, X. Lai, and D. W. Goodman, Science **281**, 1647 (1998).
[3] A. Sanchez *et al.*, J. Phys. Chem. A **103**, 9573 (1999); H. Häkkinen *et al.*, Angew. Chem., Int. Ed. **42**, 1297 (2003); B. Yoon *et al.*, Science **307**, 403 (2005).
[4] H.-J. Freund, Faraday Discuss. **114**, 1 (1999); H.-J. Freund, M. Bäumer, and H. Kuhlenbeck, Adv. Catal. **45**, 333 (2000).
[5] *Clusters of Atoms and Molecules*, edited by H. Haberland (Springer, Berlin, 1994).
[6] W. A. de Heer, Rev. Mod. Phys. **65**, 611 (1993).
[7] M. Haruta, T. Kobayashi, H. Sano, and N. Yamada, Chem. Lett. **16**, 405 (1987).
[8] N. Nilius, T. M. Wallis, and W. Ho, Science **297**, 1853 (2002).
[9] J. Lagoute, X. Liu, and S. Fölsch, Phys. Rev. Lett. **95**, 136801 (2005).
[10] A. Bettac, L. Köller, V. Rank, and K. H. Meiwes Broer, Surf. Sci. **402**, 475 (1998).
[11] H. Hövel and I. Barke, New J. Phys. **5**, 31 (2003).
[12] N. Nilius *et al.*, Phys. Rev. Lett. **100**, 096802 (2008).
[13] J. Wollschläger *et al.*, Appl. Surf. Sci. **142**, 129 (1999).
[14] S. Schintke *et al.*, Phys. Rev. Lett. **87**, 276801 (2001).
[15] G. Pacchioni, L. Giordano, and M. Baistrocchi, Phys. Rev. Lett. **94**, 226104 (2005).
[16] M. Sterrer *et al.*, Phys. Rev. Lett. **98**, 096107 (2007).
[17] P. Frondelius, H. Häkkinen, and K. Honkala, Phys. Rev. B **76**, 073406 (2007); New J. Phys. **9**, 339 (2007).
[18] M. Walter, P. Frondelius, K. Honkala, and H. Häkkinen, Phys. Rev. Lett. **99**, 096102 (2007).
[19] M. Sterrer, T. Risse, M. Heyde, H.-P. Rust, and H.-J. Freund, Phys. Rev. Lett. **98**, 206103 (2007).
[20] D. Ricci, A. Bongiorno, G. Pacchioni, and U. Landman, Phys. Rev. Lett. **97**, 036106 (2006).
[21] J. J. Mortensen, L. B. Hansen, and K. W. Jacobsen, Phys. Rev. B **71**, 035109 (2005).
[22] J. P. Perdew, K. Burke, and M. Ernzerhof, Phys. Rev. Lett. **77**, 3865 (1996).
[23] See EPAPS Document No. E-PRLTAO-102-068922 for details of the computational method. For more information on EPAPS, see http://www.aip.org/pubservs/epaps.html.
[24] G. Henkelman, A. Arnaldson, and H. Jonsson, Comput. Mater. Sci. **36**, 354 (2006).
[25] J. Tersoff and D. R. Hamann, Phys. Rev. Lett. **50**, 1998 (1983).
[26] V. Simic-Milosevic *et al.*, Phys. Rev. B **78**, 235429 (2008).
[27] The workable bias range is restricted to ± 1.3 V, as higher values induce desorption and structural changes of the Au clusters.